Plasminogen Kringle 5 blocks tumor progression by antiangiogenic and proinflammatory pathways

Sabrina R. Perri,[1] Daniel Martineau,[2] Moïra François,[3] Laurence Lejeune,[3] Louis Bisson,[4] Yves Durocher,[4] and Jacques Galipeau[1,3,5]

[1]Division of Experimental Medicine, Lady Davis Institute for Medical Research, McGill University; [2]Department of Pathology and Microbiology, Université de Montréal; [3]Lady Davis Institute for Medical Research; [4]Animal Cell Technology, Biotechnology Research Institute; and [5]Division of Hematology/Oncology, Department of Medicine, Jewish General Hospital, Montreal, Quebec, Canada

Abstract

Proteolytic processing of human plasminogen generates potent antiangiogenic peptides such as angiostatin. The plasminogen kringle 5 (K5) domain, which is distinct from angiostatin, possesses potent antiangiogenic properties on its own, which can be exploited in cancer therapy. It has been recently observed that antiangiogenic agents promote leukocyte-vessel wall interaction as part of their antitumor effect. Although we have previously shown that K5 suppresses cancer growth in tumor xenograft models, its modulation of inflammation in experimental mice with intact immune systems is unknown. To determine whether K5 possesses immune proinflammatory properties, we investigated the effects of K5 in an immune competent model of breast cancer and observed that tumor rejection is substantially reduced in nonobese diabetic/severe combined immunodeficient and BALB/c nude when compared with wild-type BALB/c mice, suggesting an important role for T-lymphoid cells in the antitumor effect of K5. Tumor explant analysis shows that K5 enhances tumor recruitment of CD3$^+$ lymphoid cells, in particular, the NKT phenotype. We also observed a significant decrease in tumor-associated microvessel length and density consistent with antiangiogenic activity. Histologic analysis of K5 tumors also revealed a robust neutrophilic infiltrate, which may be explained by the neutrophil chemotactic activity of K5 as well as its ability to promote CD64 up-regulation within the CD11b$^+$ adhesive neutrophil population. In sum, our findings confirm that the K5 protein acts as a potent angiostatic agent and possesses a novel proinflammatory role via its ability to recruit tumor-associated neutrophils and NKT lymphocytes, leading to a potent antitumor response. [Mol Cancer Ther 2007;6(2):441–9]

Introduction

Proteolytic cleavage products of plasminogen, as well as individual plasminogen kringle domains such as kringle 5 (K5), possess antiangiogenic properties whose use in cancer therapy is under much scrutiny (1–6). It has been recently proposed that an array of angiostatic agents, including plasminogen derivatives like angiostatin (7), can significantly stimulate leukocyte-vessel wall interactions *in vivo* by the up-regulation of endothelial adhesion molecules in tumor vessels (8) and may enhance anticancer immune response and allow the immune system to overcome tumor immune resistance (9). However, in the setting of experimental peritonitis, angiostatin has also been shown to behave as an anti-adhesive/anti-inflammatory substance (10). The sum of these observations readily supports the antiangiogenic properties of angiostatin in the setting of pathologic neovascularization, but its immune modulatory effects remain controversial. The plasminogen K5 domain, when used on its own, displays robust antiangiogenic properties (1–3) and will also directly lead to apoptosis of anoxic tumor cells *in vitro* (11). These features make K5 an appealing antitumor biopharmaceutical with combined antitumoral and antiangiogenic properties. Indeed, we have previously shown that genetic engineering of tumor cells for expression of K5 abolishes tumor growth *in vivo*, potently suppresses cancer-associated angiogenesis, and will inhibit recruitment of tumor-associated macrophages in an immune-deficient human tumor xenograft model (12). The latter observation suggests that K5 may possess immune modulatory properties on blood-derived immune competent cells, in keeping with the observations made by others with angiostatin. To address the question of K5 influence on immunity, we compared the biology of K5-engineered breast tumor cells in immune-defective mice as well as in tumor MHC-matched mice with normal immune systems. As expected, we find that K5 is a potent inhibitor of cancer-associated angiogenesis. However, we also observed that the antitumor effect of K5 is utterly dependent on an intact immune system, in particular on the T-lymphocyte subset, and that recruitment of polymorphonuclear cells is a dominant feature of K5 tumors. These observations provide new evidence that the K5 plasminogen derivative possesses antiangiogenic as well as immune stimulatory antitumor properties.

Materials and Methods

Cell Culture Reagents

293GPG pantropic retrovirus-packaging cell line (13) was a gift from Dr. Richard C. Mulligan (Children's Hospital, Boston, MA). Murine mammary adenocarcinoma DA/3 cell line (14) was a gift from Dr. Moulay Alaoui-Jamali (Lady Davis Institute, Montreal, Quebec, Canada).

VSV-G Pseudotyped Retroviral Vector Design, Synthesis, and Titer Assessment

The bicistronic murine retrovector pIRES-EGFP was previously generated in our laboratory (15) and contains an enhanced green fluorescent protein (EGFP). The human K5 histidine-tagged (hK5His) cDNA was ligated into pIRES-EGFP to generate phK5His-IRES-EGFP. The hK5 cDNA was histidine tagged for protein detection and purification purposes because there is no commercially available anti-human K5 antibody. VSV-G pseudotyped retroparticles encoding hK5His-IRES-EGFP were generated by tetracycline withdrawal as previously published (15, 16). Engineered retroparticles were devoid of replication-competent retrovirus as determined by GFP marker rescue assay using conditioned media from target cells. The titer of the control GFP and hK5His 293GPG single clone population was assessed as previously described (16).

Transduction of Murine Mammary DA/3 Cells

DA/3 cells were transduced with hK5His-expressing retroviral particles as previously described (15). Stably transduced DA/3 cells were culture expanded and sorted to obtain polyclonal populations based on GFP expression using a Becton Dickinson FACSTAR sorter.

Characterization of Gene-Modified DA/3 Cells

Conditioned medium was collected from confluent DA/3-GFP control and hK5His-GFP–transduced DA/3 cells, concentrated, and detected by anti-His immunoblot analysis as previously described (12). The proliferation rate of gene-modified hK5His-GFP–expressing and control GFP-expressing DA/3 cells was monitored every 24 h for 4 days. Live cells were counted using trypan blue staining. The cell cycle profile of gene-modified hK5His-GFP–expressing and control GFP-expressing DA/3 cells was assessed. Cells were trypsinized, centrifuged into a pellet, washed twice with ice-cold PBS, and fixed in 70% ethanol at $-20°C$ overnight. For cell cycle analysis, the cells were washed twice with ice-cold PBS and resuspended in propidium iodide buffer (PBS, 0.1% Triton X-100, 0.1 mmol/L EDTA, 0.05 mg/mL RNase A, and 50 μmol/L propidium iodide). After 30 min of incubation at room temperature, the cell cycle distribution was determined by flow cytometry FACSCalibur (Beckman Coulter, Fullerton, CA) and analyzed using the CellQuest software (BD, Franklin Lakes, NJ). The proportion of cells in the hypodiploid (sub-G_1) area was considered to be apoptotic.

In vivo Matrigel Assay and Analysis of Cellular Infiltrate by Cytometry

Culture-expanded DA/3-GFP and DA/3-hK5His-GFP cells were aliquoted to create 50-μL cell suspensions containing 10^6 cells, mixed with 500 μL Matrigel (a semisolid matrix derived from a murine sarcoma cell line; BD Biosciences, San Jose, CA) at 4°C, and implanted s.c. in the right lateral flank of 6-week-old immunocompetent BALB/c mice (The Jackson Laboratory, Quebec, Canada). Three days after implantation, mice were sacrificed, and implants were excised and processed as previously described (17). To determine the explant cellular infiltrate, cell suspensions were stained with the following antibodies: purified rat anti-mouse CD16/CD32 (mouse Fc block) followed by APC-conjugated rat anti-mouse CD45, APC-conjugated rat anti-mouse CD3, phycoerythrin-conjugated rat anti-mouse CD4, phycoerythrin-Cy7–conjugated rat anti-mouse CD25, FITC-conjugated rat anti-mouse CD8, phycoerythrin-conjugated rat anti-mouse NKT/NK, and their corresponding isotypic controls. All antibodies were purchased from BD PharMingen (San Diego, CA). Cells were fixed with 1% paraformaldehyde, and events were acquired using a FACSCalibur flow cytometer (Beckman Coulter) and analyzed using the CellQuest software (BD).

Matrigel Explant Histochemistry

Mice were sacrificed; implants were excised, fixed in formalin, and embedded in paraffin; and 4-μm sections were prepared to generate representative sections of the border and central regions of the explants. Sections were either stained with H&E or underwent an antigen retrieval process using two microwave boils in a 10 mmol/L sodium citrate buffer (pH 6) solution. Endogenous biotin activity was blocked using a kit (Zymed Laboratories, Markham, Ontario, Canada), and sections were subsequently blocked with 2.5% bovine serum albumin in PBS and incubated with a rabbit polyclonal raised against murine von Willebrand factor (Neomarkers, Fremont, CA; dilution, 1:100) overnight. After three washes, the sections were incubated with biotinylated goat anti-rabbit IgG antibody (BD PharMingen; dilution, 1:200) for 2 h, washed, and incubated with streptavidin-peroxidase (Vector Labs, Burlingame, CA) for 1 h before the addition of 3,3′-diaminobenzidine chromogenic substrate (Vector Labs). Meyer's hematoxylin was used for counterstaining. The microvessel length was measured on 30 randomly selected von Willebrand factor–positive vessels from each experimental group using an ocular and stage micrometer. The microvessel density was calculated by counting all von Willebrand factor–positive vessels on three randomly selected sections from each group using a Leica light microscope (Leica Microsystems, Inc., Richmond Hill, Ontario, Canada) at ×400 magnification and dividing by the total section surface area. The mean number of von Willebrand factor–positive blood vessels per mm^2 was plotted.

Production of Purified K5 Protein

Serum-free and suspension-growing human embryonic kidney 293 cell line stably expressing EBNA1 was transiently transfected in a shaker flask with hK5His-containing pTT expression vector essentially as previously described (18). Conditioned media was collected 120 h after transfection, concentrated, and purified using an immobilized metal-affinity chromatography system (Novagen, La

Jolla, CA). Eluted protein fractions were analyzed by anti-His immunoblot. Semiquantitative anti-His immunoblot was done to quantify the amount of K5 protein (data not shown).

Neutrophil Isolation

Heparinized whole blood (50 mL) was collected from a healthy human donor, layered over a Ficoll-density gradient, and centrifuged at 1,600 rpm for 30 min. The polymorphonuclear neutrophil (PMN)–rich fraction was collected and resuspended in 0.9% NaCl. RBC were lysed by exposure to cold 0.2% NaCl for 30 s followed by neutralization with cold 1.6% NaCl and spun at 1,000 rpm for 5 min. Lysis steps were repeated until RBC fraction was removed. Calcein AM (Molecular Probes, Eugene, OR; 10 mg/mL) was added to a 5-mL PMN suspension in HBSS, and cells were incubated for 30 min at 37°C. PMN were then washed twice with PBS, counted, and resuspended in Opti-MEM to the desired concentration.

Fluorescence-Based PMN Migration Assay

A 96-well, 3-μm pore size chemotaxis chamber (ChemoTx, Neuro Probe, Gaithersburg, MD) was used, and the migration assay was done as described by Frevert et al. (19). Briefly, the bottom chambers were filled with 29 μL of either increasing concentrations of purified hK5His protein (80–160 ng) diluted in Opti-MEM or Opti-MEM alone as a negative control. To determine the total fluorescence of PMN added to the top side of the filter, 25 μL of each cell suspension (0, 0.25, 0.5, 1.0, 2.0 3.0, and 5.0×10^6 PMN/mL) was placed directly in duplicate wells in the bottom chamber. The polycarbonate filters were positioned on the loaded microplate and secured in place with corner pins. PMNs (7.5×10^4, 50 μL) were placed directly onto the filter sites, and the chamber was incubated for 7 h at 37°C. The nonmigrating cells on the top side of the filter were removed by gently wiping the filter with a tissue. The chemotaxis filter was placed in a FLUOstar OPTIMA fluorescent plate reader (Fisher Scientific, Ottawa, Ontario, Canada), and the cells that migrated into the bottom chamber were measured by using the calcein fluorescence signal. The fluorescent plate reader was configured in order for the probe to be in a bottom-read position, which allows for detection of fluorescence in each well of the chemotaxis chamber (excitation, 485 nm; emission, 530 nm).

Cell Staining

PMNs were exposed to increasing doses of purified hK5His protein (80, 120, or 160 ng) diluted in Opti-MEM or Opti-MEM alone as a negative control or phorbol myristate acetate as a positive control for 2 h at 37°C. PMNs were then costained with phycoerythrin-labeled anti-human CD11b antibody and biotin-labeled anti-human CD64 antibody. Gene-modified DA/3 cells were stained with biotin-conjugated anti-H-2Kd (MHC-I) antibody. The biotinylated antibody was revealed using APC-streptavidin. Antibodies were purchased from BD PharMingen. Cells were fixed with 1% paraformaldehyde, and events were acquired using a FACSCalibur flow cytometer (Beckman Coulter) and analyzed using the CellQuest software (BD).

Results

DA/3 Mouse Mammary Tumor Cell Line Retrovirally Engineered to Express Plasminogen K5 Domain

The hK5His cDNA was cloned as previously described (12) into a bicistronic retroviral vector construct (ref. 15; Fig. 1A). The hK5His retrovector plasmid was stably transfected into 293GPG retroviral packaging cells, and retrovirus producer cells were selected as described in Materials and Methods. Tetracycline withdrawal from the culture media led to the production of VSVG-typed hK5His-GFP retroviral particles, which were subsequently concentrated 100-fold by ultracentrifugation, and a viral titer of $\sim 2.5 \times 10^6$ infectious particles/mL was obtained. Concentrated VSVG-typed hK5His-GFP retroviral particles were used to transduce the BALB/c-compatible DA/3 murine mammary cancer cell line. The DA/3 murine mammary adenocarcinoma cell line is estrogen independent and serves as a murine model of locally advanced breast cancer (14, 20–22). Following retroviral transduction, polyclonal gene-modified DA/3 cells were assessed for GFP expression by flow cytometry and sorted to obtain a 100% GFP-positive population. To ensure hK5His transgene expression and proper secretion, anti-His immunoblot analysis was done on conditioned supernatant collected from hK5His-transduced murine DA/3 mammary tumor cells and detects a major 15,000-Dalton protein consistent with the predicted molecular weight of soluble hK5His (Fig. 1B). Using a semiquantitative Western blot titration curve, it was estimated that hK5His-GFP–expressing DA/3 cells secrete 0.02 pmol/L (or 0.25 ng) of soluble hK5His protein per 10^6 cells per 24 h (data not shown). Expression of hK5His protein did not alter the proliferation rate or the cell cycle profile of hK5His-expressing DA/3 cells compared with control DA/3 cells (Fig. 1C and D).
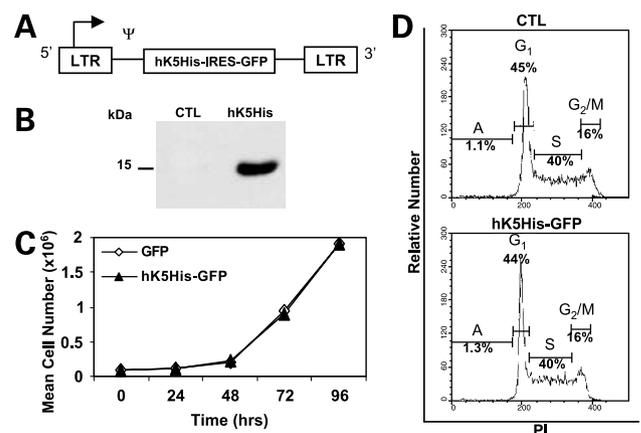

Figure 1. Development and characterization of hK5His-GFP gene–modified DA/3 cells. **A,** hK5His retrovector when integrated in DA/3 cells. **B,** anti-His immunoblot analysis reveals functional secretion of hK5His migrating at $\sim$15 kDa from retrovirally gene-modified DA/3 cells. **C,** proliferation rate of hK5His-GFP–expressing DA/3 cells is equivalent to that of GFP-expressing DA/3 cells ($P > 0.05$). **D,** representative example of the cell cycle profile of control and hK5His-GFP–expressing DA/3 cells. Percentage of cells in A or apoptotic (or sub-G_1), G_1, S, and G_2-M.

Antitumor Property of hK5His Protein Is Dependent Upon an Intact Immune System

We tested the efficacy of hK5His against breast cancer in mice with functional immune systems. DA/3, genetically engineered DA/3-GFP, or DA/3-hK5His-GFP polyclonal cells were implanted s.c. in immune competent BALB/c mice, and animal survival was monitored over time. One year after implantation, 65% of hK5His-GFP–implanted mice survived tumor-free ($P < 0.0001$) compared with 20% in both DA/3- and DA/3-GFP–implanted control mice (Fig. 2A). The antitumor effect was severely diminished when genetically engineered DA/3-GFP or DA/3-hK5His-GFP polyclonal cells were implanted s.c. in immunodeficient nonobese diabetic/severe combined immunodeficient mice (Fig. 2B). This mouse strain lacks functional endogenous T or B lymphocytes due to a deficiency in the *recombinase activating gene-2* (*RAG-2*) gene, which impairs rearrangement of separate gene elements of the immunoglobulin and T-cell antigen receptor genes and thus disrupts differentiation of both B- and T-lymphocyte progenitor cells (23). Although hK5His-GFP–implanted mice succumbed to excessive tumor burden by 2 months after implantation, their survival was significantly prolonged compared with control mice ($P < 0.0001$), possibly due to the angiostatic property of hK5His protein. This observation suggests that the immune system is playing a role in the tumoricidal effects of hK5His protein. We proceeded to test whether the immune modulatory effect of hK5His protein was mediated via T lymphocytes by s.c. implanting DA/3-GFP or DA/3-hK5His-GFP polyclonal cells in athymic BALB/c nude (T-lymphocyte deficient) mice (Fig. 2C). Our results show that T lymphocytes are required for hK5His protein to exert its antitumor action because all hK5His-GFP–implanted mice had to be sacrificed due to tumor development by 3 months after implantation, albeit delayed survival compared with GFP-implanted control mice ($P < 0.0005$). To assess if hK5His protein elicited an adaptive systemic protective immune response, we s.c. implanted wild-type BALB/c mice with irradiated DA/3-GFP or DA/3-hK5His-GFP cells and, 14 days later, challenged the mice on the opposite flank with non-irradiated DA/3-GFP cells (Fig. 2D). Protective immunity was not observed because there was no significant difference between the survival rate of challenged GFP-implanted and hK5His-GFP–implanted mice ($P = 0.37$).
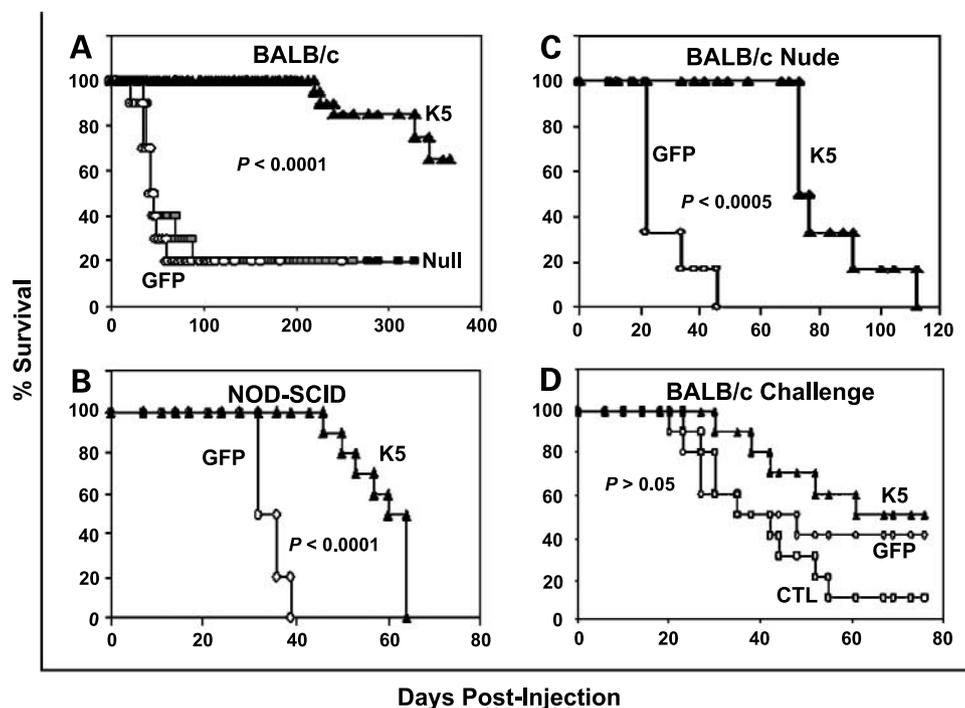
Figure 2.   hK5His-GFP–implanted immunocompetent mice survive long term and modulate the immune system to suppress tumor growth. Kaplan-Meier long-term survival of (**A**) immunocompetent BALB/c mice implanted s.c. with 10^6 non–gene-modified DA/3 ($n = 10$), GFP-expressing DA/3 ($n = 10$), or hK5His-GFP–expressing DA/3 cells ($n = 10$). Mice were sacrificed upon severe tumor ulceration with a typical tumor volume > 500 mm^3. Surviving mice had no measurable tumor. The experiment was done twice with similar results. Kaplan-Meier survival of (**B**) nonobese diabetic/severe combined immunodeficient (*NOD-SCID*) mice and (**C**) athymic BALB/c nude mice implanted s.c. with 10^6 GFP-expressing DA/3 ($n = 10$ and $n = 6$, respectively) and hK5His-GFP–expressing DA/3 cells ($n = 10$ and $n = 6$, respectively). **D,** Kaplan-Meier survival of immunocompetent BALB/c mice implanted s.c. with irradiated 5×10^5 GFP-expressing DA/3 (*GFP*; $n = 10$) or hK5His-GFP–expressing DA/3 cells (*K5*; $n = 10$) and challenged 14 d later (day 0 on graph) on the opposite flank with 5×10^5 non-irradiated GFP-expressing DA/3 cells. BALB/c mice (*CTL*; $n = 10$) were independently implanted s.c. with 5×10^5 non-irradiated GFP-expressing DA/3 cells on the same day as the challenge as a technical control to show the tumor growth potential. Log-rank statistical test was done for all Kaplan-Meier graphs.
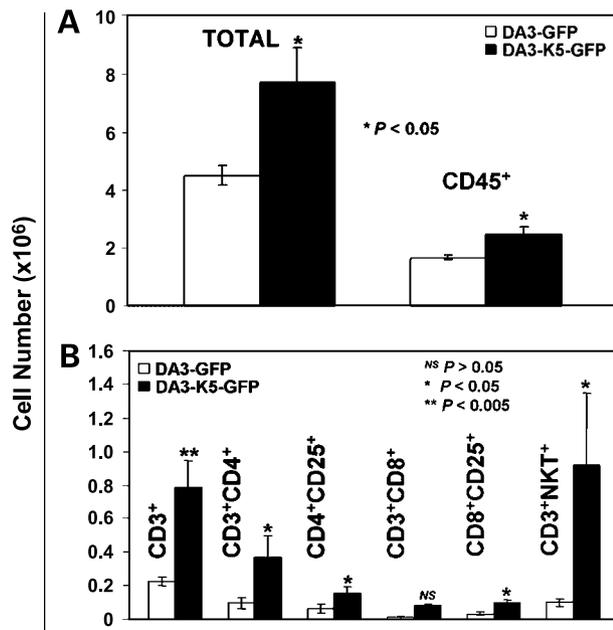
Figure 3. hK5His possesses novel immunostimulatory property. **A,** absolute total cell count was done after collagenase digestion of the explants 3 d after implantation of 10^6 GFP-expressing DA/3 ($n = 4$) or hK5His-GFP–expressing DA/3 cells ($n = 4$) embedded in Matrigel. *Columns,* absolute number of infiltrated CD45$^+$ hematopoietic cells; *bars,* SE. **B,** *columns,* absolute number of infiltrated lymphoid cells: CD3$^+$, CD3$^+$CD4$^+$, CD4$^+$CD25$^+$, CD3$^+$CD8$^+$, CD8$^+$CD25$^+$, CD3$^+$NKT$^+$; *bars,* SE. Statistical analysis was done using Student's *t* test.

hK5His Protein Expression by DA/3 Cells Leads to Recruitment of CD3$^+$ Lymphocytes *In vivo*

To further characterize the immune cellular mediators involved in hK5His protein antitumor effect, we embedded DA/3-GFP or DA/3-hK5His-GFP polyclonal cells in Matrigel and s.c. implanted the cells in immunocompetent BALB/c mice. Implants were retrieved 3 days after implantation and collagenase digested to obtain a single-cell suspension. Cells in each experimental group were counted using a hemacytometer, and the cellular infiltrate was analyzed by staining the single-cell suspension with four-color antibodies enabling the identification of different immune subsets by flow cytometry analysis. Our infiltrate analysis confirms that hK5His protein secreted by gene-engineered DA/3 cells induces a potent host-derived cellular infiltrate, including CD45$^+$ hematopoietic cells (Fig. 3A). T-lymphoid subset analysis (Fig. 3B) shows a substantial increase in the absolute number of infiltrated CD3$^+$ lymphocytes ($P < 0.005$), in particular CD3$^+$NKT$^+$ cells ($P < 0.05$).

hK5His Protein Expression by DA/3 Cells Influences the Quantity and Size of Tumor-Associated Microvasculature

We have previously shown that hK5His secretion by human glioma cells leads to a profound antiangiogenic effect in nonobese diabetic/severe combined immunodeficient mice (12). To test whether this effect was replicated in

immune competent BALB/c mice and could also be used to explain in part the observed prolonged survival in hK5His-GFP–implanted immune deficient mice, we embedded DA/3, DA/3-GFP, or DA/3-hK5His-GFP polyclonal cells in Matrigel and s.c. implanted the cells in BALB/c mice. One week after implantation, the Matrigel plugs were retrieved (Fig. 4A), sectioned, and stained with von Willebrand factor antibody (Fig. 4B, *left*). The number (Fig. 4C) as well as the length (Fig. 4B, *right*) of blood vessels were significantly reduced in the hK5His plugs, consistent with a potent antiangiogenic effect *in vivo*.

hK5His Induces Neutrophilic Tumor Infiltration

In an effort to understand the effect of hK5His on host-derived inflammation, we embedded DA/3, DA/3-GFP, or DA/3-hK5His-GFP polyclonal cells in Matrigel and s.c. implanted the cells in immunocompetent BALB/c mice.
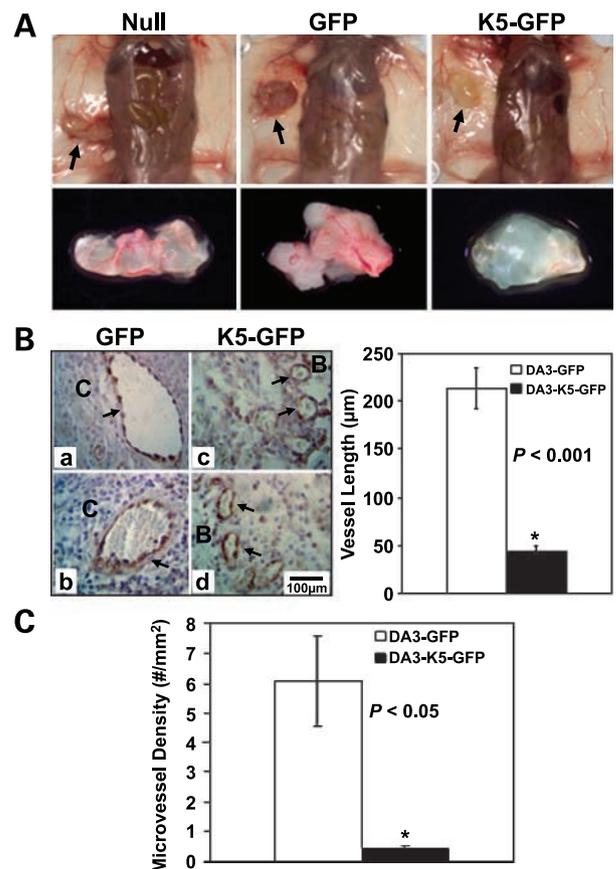
Figure 4. hK5His acts as a potent antiangiogenic agent. **A,** implant (*arrow*) retrieval 1 wk after implantation of 10^6 Matrigel: embedded DA/3 ($n = 4$), DA/3-GFP ($n = 4$), or DA/3-hK5His-GFP ($n = 4$) cells (representative images at the same magnification). **B,** *left,* representative images of von Willebrand factor–positive immunostained blood vessels (*black arrows*) from two different DA/3-GFP–containing (**a** and **b**) and DA/3-hK5His-GFP–containing (**c** and **d**) implants. *C,* center of implant. *B,* border of implant. Magnification, ×160. *Right, columns,* mean von Willebrand factor–positive vessel length (μm) for both experimental groups; *bars,* SE. **C,** *columns,* mean number of von Willebrand factor–positive blood vessels divided by the mean section surface area (microvessel density; mm^2); *bars,* SE. Statistical analysis was done using Student's *t* test.
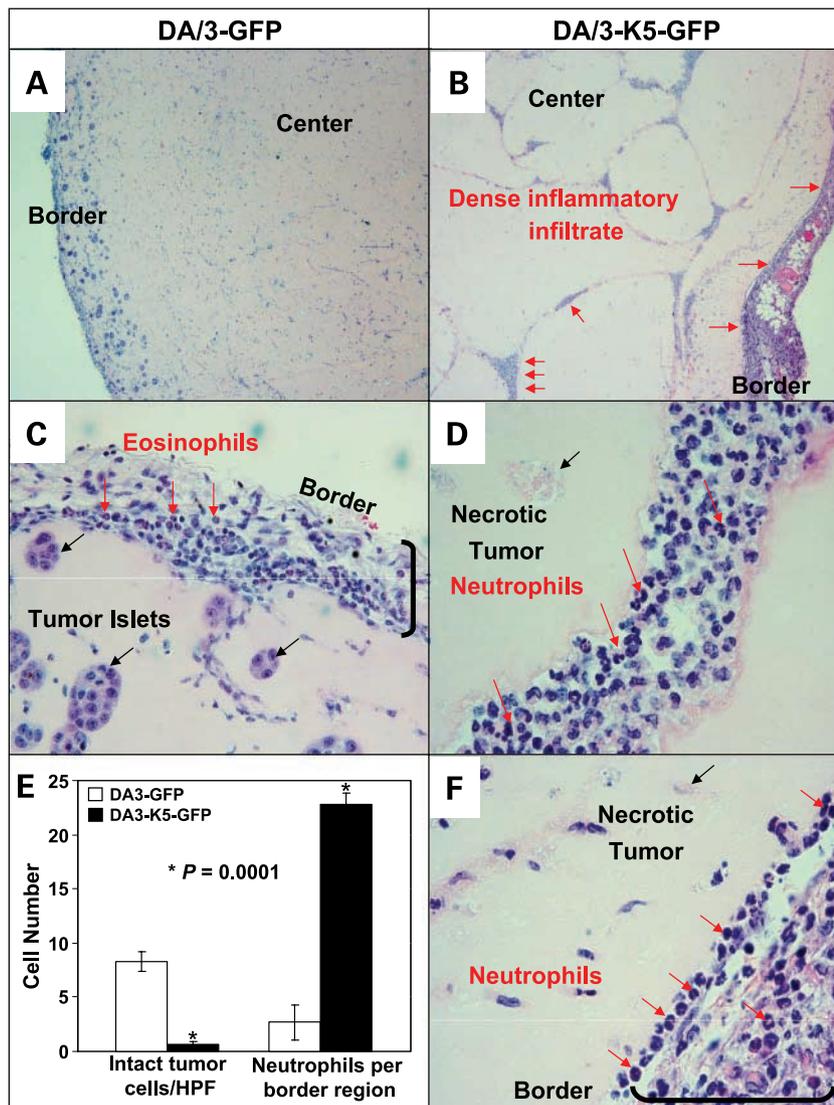
Figure 5. hK5His protein induces dense pericapillary neutrophilic infiltrate. H&E-stained Matrigel explant sections retrieved 3 d after implantation, containing either GFP-expressing ($n = 4$) DA/3 cells (**A**, ×2.5 and **C**, ×20) or hK5His-GFP–expressing ($n = 4$) DA/3 cells (**B**, ×2.5; **D**, ×40; and **E**, ×40). **B,** inflammatory infiltrate (*red arrows*). **C,** eosinophils present along the border region (*red arrows*) and tumor islets composed of six cells (*black arrows*). **D** and **F,** neutrophils within the center region and within the border capsule region (*red arrows*) and representative examples of necrotic tumors (*black arrows*). **E,** *columns,* mean quantitative histologic analysis representing the number of intact tumor cells per high power field (*left*) and the number of neutrophils per border region (*right*) composed of concentric layers of edematous immature connective tissue; *bars,* SE. Statistical analysis was done using Student's *t* test.

Implants were retrieved 3 days after implantation, sectioned, stained with H&E, and analyzed by a veterinary pathologist (coauthor: D.M.). The histologic analysis revealed that there were almost no intact islet (acini) of tumor cells in the hK5His-containing implants compared with the GFP-containing implants (Fig. 5E; $P = 0.0001$), where there was a moderate number of islets, sometimes acini, of intact tumor cells present at the periphery of the implants as seen in Fig. 5A and C. The DA/3-hK5His-GFP tumor cells occurred as single cells, rarely in pairs, in contrast with the DA/3-GFP tumor cells that occurred in islets of at least six cells. Most of the DA/3-hK5His-GFP tumor cells observed were either necrotic or degenerated (Fig. 5D and F) and were often surrounded by inflammatory cells compared with the DA/3-GFP tumor cells that seemed healthy. Both GFP- and hK5His-GFP–containing implants were incompletely surrounded by a capsule at the border regions (Fig. 5C and F, respectively) composed of concentric layers of edematous immature connective tissue. We observed that the hK5His-GFP–containing implants were markedly thickened by a dense population of inflammatory cells (Fig. 5B and D) composed of at least 50% neutrophils, qualified as suppurative inflammation. Enumeration confirmed a substantial increase in the number of infiltrated neutrophils in the hK5His-GFP–containing implants compared with the control implants (Fig. 5E; $P = 0.0001$). There were several eosinophils in the border zone of both groups. However, there was no significant difference in the number of infiltrated eosinophils between test and control (data not shown).

hK5His Protein Is Chemotactic for Neutrophils and Promotes Their Activation

To explain the enhanced recruitment of host-derived neutrophils within the hK5His-GFP–containing implants, we assessed the ability of soluble hK5His protein to act as a neutrophil chemoattractant. PMN isolated from

heparinized human peripheral blood as described in Materials and Methods were assayed for cell surface expression of the adhesion marker CD11b (Mac-1) by flow cytometry analysis and were found to be strongly positive (Fig. 6A). PMN were plated on the top surface of the migration filter and exposed to either increasing doses of purified hK5His protein diluted in Opti-MEM or Opti-MEM alone as a control. We observed that hK5His protein acts as a potent neutrophil chemoattractant and displays a dose-response effect (Fig. 6B). Additionally, we show that neutrophil exposure to soluble hK5His protein induces increased cell surface expression of the granulocyte activation marker CD64 (Fcγ receptor I) within the CD11b^{+} (Mac-1) adhesive neutrophil subset (Fig. 6C). These findings are consistent with our histologic analysis and suggest that soluble hK5His protein produced by gene-modified DA/3 cells acts as a strong neutrophil chemoattractant and promotes activation of neutrophils within the tumor microenvironment.

MHC-I Expression in hK5His-Expressing DA/3 Cells

MHC-I is a key molecule involved in immune surveillance, and its level of expression may influence interaction with innate effectors (24–27). Therefore, we ascertained whether hK5His altered this phenotype. We assessed the cell surface expression of MHC class I antigen on GFP- and hK5His-GFP–expressing DA/3 cells by flow cytometry. Our results indicate that hK5His-GFP–expressing DA/3 cells express similar levels (54.4%) of MHC-I (H-2Kd) molecule as GFP-expressing DA/3 cells (64.1%; $P > 0.05$; data not shown).

Discussion

We have previously shown that tumor-expressed hK5His leads to a substantial antiangiogenic effect and cure of human glioma orthotopic xenografts in a majority of athymic *nu/nu* nude mice (12). We observed that hK5His protein acts as a potent antiangiogenic agent via its inhibition of tumor-derived endothelial cells and tumor-associated macrophages. In the current study, we observed that nonobese diabetic/severe combined immunodeficient and athymic nude BALB/c mice with impaired T-lymphoid immune systems do not mount as effective an antitumor response to DA/3 cells expressing hK5His, when compared with immunologically normal rodents. Furthermore, despite apparent long-term cures lasting more than 1 year in normal BALB/c mice, we were unable to show an effective adaptive immune response to tumor challenge, suggesting that components of the innate immune system play an important role in the effectiveness of K5 antitumor properties (Fig. 2). These observations are congruent with the hypothesis that antiangiogenic compounds derived from plasminogen and other sources have pleiotropic effects, which likely involve a synergistic recruitment of an inflammatory antitumor response (8, 9). We have observed that tumor expression of hK5His leads to a robust CD3^{+} lymphoid tumor infiltration, in particular NKT cells, suggesting a role for these immune effector cells in

K5-mediated tumor rejection (Fig. 3). Histologic examination of tumor implants confirmed a robust suppression of cancer neovascularization (Fig. 4) and a marked neutrophilic suppurative reaction (Fig. 5). This neutrophilic infiltration may be mediated by soluble K5 protein, which we show acts as a chemoattractant for neutrophils and promotes up-regulation of the CD64 granulocyte activation marker (Fig. 6). This observation follows in the stead of the recently discovered property of an array of antiangiogenic pharmaceuticals, including plasminogen derivatives such as angiostatin, to alter the phenotype of cancer-associated neovasculature in a manner that leads to enhanced tumor recruitment of leukocytes. Dirkx et al. recently reported that a synthetic angiogenesis inhibitor (anginex) enhances leukocyte-vessel wall interactions in tumor vessels by up-regulating tumor endothelial VCAM-1 and E-selectin expression and subsequently increases infiltration of CD45^{+} leukocytes and cytotoxic CD8^{+} lymphocytes into the tumor to suppress tumor growth (8). Although Dirkx et al. report that angiostatin can also increase the leukocyte-vessel wall interaction *in vivo*, Chavakis et al. claim that angiostatin acts as an anti-adhesive and anti-inflammatory agent because it inhibits peritonitis-induced neutrophil
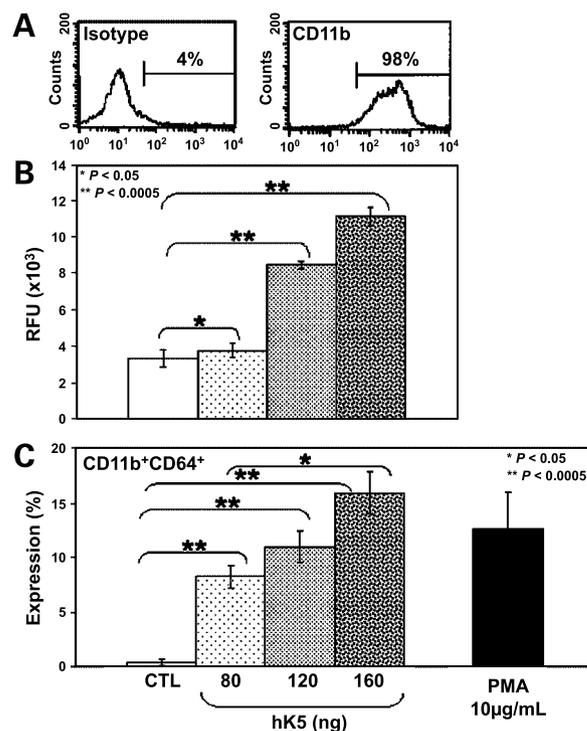
Figure 6. hK5His protein acts as a neutrophil chemoattractant and promotes activation. **A,** expression of CD11b cell surface adhesion marker on isolated PMN: isotype antibody (*left*) and test antibody (*right*). **B,** relative fluorescence units (*RFU*) of migrated PMN toward either increasing doses of purified hK5His protein (80, 120, and 160 ng) diluted in Opti-MEM or Opti-MEM alone. **C,** *columns,* mean % expression of CD11b^{+}CD64^{+} PMN after exposure to either increasing doses of purified hK5His protein (80, 120, and 160 ng) diluted in Opti-MEM or Opti-MEM alone or phorbol myristate acetate (*PMA*; 10 μg/mL) as a positive control; *bars,* SE. Statistical analysis was done using Student's *t* test.

emigration *in vivo* via its interaction with $\alpha_4\beta_1$ integrin and Mac-1 ($\alpha_M\beta_2$ integrin; ref. 10). These reports provide a premise for the immune modulatory activity of plasminogen kringle fragments, such as angiostatin, where its capacity to promote or prevent immune effectors varies with the disease model system. Our observation that K5 enhances recruitment of NKT cells and neutrophils is in support of a proinflammatory mode of action and buttresses the theory that inflammation and microvascular suppression act synergistically in the observed antitumor effects of hK5. Our survival data in both immunodeficient nonobese diabetic/severe combined immunodeficient and BALB/c nude mice show that although host-derived neutrophils may be implicated in suppressing tumor progression, their presence is not sufficient in T-cell deficient mice to eradicate the tumor, suggesting a cooperative antitumor effect between these immune effector cells. There is precedence for combined lymphocytic and neutrophilic involvement in tumor rejection. Cairns et al. (28) reported that gene-engineered myeloma cells expressing lymphotactin induced infiltration of CD4^{+}, CD8^{+}, and neutrophils, leading to effective tumor regression *in vivo*. Lee et al. (29) described that *in vivo* injection of interleukin-8–transfected human ovarian cancer cells induced dramatic neutrophilic infiltration and resulted in decreased tumor growth. In the context of antiangiogenic therapy, Pike et al. (30) also observed *in vivo* neutrophilic and lymphocytic infiltration in vasostatin (angiogenic inhibitor)–treated Burkitt lymphoma tumors, which led to tumor suppression.

Work from Abbott Laboratories shows that cancer cells rendered anoxic *in vitro* translocate GRP78 to the cell membrane, which then serves as a ligand for K5. K5-bound GRP78 thereafter initiates an apoptotic cascade (11). The significance of this phenomenon was not tested in experimental animals; however, it clearly buttresses the claim that K5 can directly affect the phenotype and cellular function of tumor cells. We did not observe an increased apoptosis index or reduced cell growth of K5-expressing DA/3 cells in standard tissue culture conditions or in a 3% oxygen hypoxic environment, nor were we able to detect membrane-bound GRP78 despite its intracellular abundance in DA/3 cells (data not shown). These observations suggest that K5 likely interacts with tumor cells via a plurality of pathways, of which GRP78 may be one in certain circumstances. Thus, it may be speculated that hK5His protein breaks immune tolerance by inducing a cross-talk to occur between host-derived neutrophils and other innate infiltrating immune cells such as NKT lymphocytes. Furthermore, K5 from DA/3 may lead to an altered adhesive phenotype of tumor-associated vessels and promote local recruitment of leukocytes from the bloodstream.

In aggregate, our data confirm the antiangiogenic potency of hK5His and suggest that hK5His protein also relies upon multiple innate cellular effectors to induce its *in vivo* antineoplastic effect. More specifically, our findings show that hK5His protein requires functional neutrophils and T lymphocytes to induce optimal tumor rejection. Further studies on the pleiotropic effects of K5 protein on vasculature and inflammatory effector cells may provide new insights, allowing K5 to be therapeutically exploited to treat cancer.

References

1. Cao Y, Ji RW, Davidson D, et al. Kringle domains of human angiostatin. Characterization of the anti-proliferative activity on endothelial cells. J Biol Chem 1996;271:29461 – 7.

2. Cao Y, Chen A, An SS, Ji RW, Davidson D, Llinas M. Kringle 5 of plasminogen is a novel inhibitor of endothelial cell growth. J Biol Chem 1997;272:22924 – 8.

3. Cao Y, Cao R, Veitonmaki N. Kringle structures and antiangiogenesis. Curr Med Chem Anti-Canc Agents 2002;2:667 – 81.

4. Chang Y, Mochalkin I, McCance SG, Cheng B, Tulinsky A, Castellino FJ. Structure and ligand binding determinants of the recombinant kringle 5 domain of human plasminogen. Biochemistry 1998;37:3258 – 71.

5. Geiger JH, Cnudde SE. What the structure of angiostatin may tell us about its mechanism of action. J Thromb Haemost 2004;2:23 – 34.

6. Soff GA. Angiostatin and angiostatin-related proteins. Cancer Metastasis Rev 2000;19:97 – 107.

7. O'Reilly MS, Holmgren L, Shing Y, et al. Angiostatin: a novel angiogenesis inhibitor that mediates the suppression of metastases by a Lewis lung carcinoma. Cell 1994;79:315 – 28.

8. Dirkx AE, oude Egbrink MG, Castermans K, et al. Anti-angiogenesis therapy can overcome endothelial cell anergy and promote leukocyte-endothelium interactions and infiltration in tumors. FASEB J 2006;20: 621 – 30.

9. Sun X, Kanwar JR, Leung E, Lehnert K, Wang D, Krissansen GW. Angiostatin enhances B7.1-mediated cancer immunotherapy independently of effects on vascular endothelial growth factor expression. Cancer Gene Ther 2001;8:719 – 27.

10. Chavakis T, Athanasopoulos A, Rhee JS, et al. Angiostatin is a novel anti-inflammatory factor by inhibiting leukocyte recruitment. Blood 2005; 105:1036 – 43.

11. Davidson DJ, Haskell C, Majest S, et al. Kringle 5 of human plasminogen induces apoptosis of endothelial and tumor cells through surface-expressed glucose-regulated protein 78. Cancer Res 2005;65: 4663 – 72.

12. Perri SR, Nalbantoglu J, Annabi B, et al. Plasminogen kringle 5-engineered glioma cells block migration of tumor-associated macrophages and suppress tumor vascularization and progression. Cancer Res 2005;65: 8359 – 65.

13. Ory DS, Neugeboren BA, Mulligan RC. A stable human-derived packaging cell line for production of high titer retrovirus/vesicular stomatitis virus G pseudotypes. Proc Natl Acad Sci USA 1996;93: 11400 – 6.

14. Medina D. Mammary tumorigenesis in chemical carcinogen-treated mice. VI. Tumor-producing capabilities of mammary dysplasias in BALB/cCrgl mice. J Natl Cancer Inst 1976;57:1185 – 9.

15. Galipeau J, Li H, Paquin A, Sicilia F, Karpati G, Nalbantoglu J. Vesicular stomatitis virus G pseudotyped retrovector mediates effective *in vivo* suicide gene delivery in experimental brain cancer. Cancer Res 1999;59:2384 – 94.

16. Eliopoulos N, Galipeau J. Green Fluorescent Protein. In: Hicks BW, editor. Totowa: Humana Press, Inc.; 2002. p. 353 – 71.

17. Stagg J, Lejeune L, Paquin A, Galipeau J. Marrow stromal cells for interleukin-2 delivery in cancer immunotherapy. Hum Gene Ther 2004;15: 597 – 608.

18. Durocher Y, Perret S, Kamen A. High-level and high-throughput recombinant protein production by transient transfection of suspension-growing human 293-EBNA1 cells. Nucleic Acids Res 2002;30:E9.

19. Frevert CW, Wong VA, Goodman RB, Goodwin R, Martin TR. Rapid fluorescence-based measurement of neutrophil migration *in vitro*. J Immunol Methods 1998;213:41 – 52.

20. Matory YL, Chen M, Goedegebuure PS, Eberlein TJ. Anti-tumor effects and tumor immunogenicity following IL2 or IL4 cytokine gene transfection of three mouse mammary tumors. Ann Surg Oncol 1995;2: 502 – 11.

21. Matory YL, Chen M, Dorfman DM, Williams A, Goedegebuure PS, Eberlein TJ. Antitumor activity of three mouse mammary cancer cell lines after interferon-gamma gene transfection. Surgery 1995;118:251 – 5.

22. Baruch A, Hartmann M, Zrihan-Licht S, et al. Preferential expression of novel MUC1 tumor antigen isoforms in human epithelial tumors and their tumor-potentiating function. Int J Cancer 1997;71:741 – 9.

23. Prochazka M, Gaskins HR, Shultz LD, Leiter EH. The nonobese diabetic scid mouse: model for spontaneous thymomagenesis associated with immunodeficiency. Proc Natl Acad Sci USA 1992;89:3290 – 4.

24. Karre K. NK cells, MHC class I molecules and the missing self. Scand J Immunol 2002;55:221 – 8.

25. Levitsky HI, Lazenby A, Hayashi RJ, Pardoll DM. *In vivo* priming of two distinct antitumor effector populations: the role of MHC class I expression. J Exp Med 1994;179:1215 – 24.

26. Moron G, Dadaglio G, Leclerc C. New tools for antigen delivery to the MHC class I pathway. Trends Immunol 2004;25:92 – 7.

27. Trombetta ES, Mellman I. Cell biology of antigen processing *in vitro* and *in vivo*. Annu Rev Immunol 2005;23:975 – 1028.

28. Cairns CM, Gordon JR, Li F, Baca-Estrada ME, Moyana T, Xiang J. Lymphotactin expression by engineered myeloma cells drives tumor regression: mediation by CD4^{+} and CD8^{+} T cells and neutrophils expressing XCR1 receptor. J Immunol 2001;167:57 – 65.

29. Lee LF, Hellendall RP, Wang Y, et al. IL-8 reduced tumorigenicity of human ovarian cancer *in vivo* due to neutrophil infiltration. J Immunol 2000;164:2769 – 75.

30. Pike SE, Yao L, Jones KD et al. Vasostatin, a calreticulin fragment, inhibits angiogenesis and suppresses tumor growth. J Exp Med 1998;188:2349 – 56.

Plasminogen Kringle 5 blocks tumor progression by antiangiogenic and proinflammatory pathways

Sabrina R. Perri, Daniel Martineau, Moïra François, et al.

Updated version	Access the most recent version of this article at: http://mct.aacrjournals.org/content/6/2/441

Cited articles	This article cites 28 articles, 12 of which you can access for free at: http://mct.aacrjournals.org/content/6/2/441.full#ref-list-1
Citing articles	This article has been cited by 1 HighWire-hosted articles. Access the articles at: http://mct.aacrjournals.org/content/6/2/441.full#related-urls

E-mail alerts	Sign up to receive free email-alerts related to this article or journal.
Reprints and Subscriptions	To order reprints of this article or to subscribe to the journal, contact the AACR Publications Department at pubs@aacr.org.
Permissions	To request permission to re-use all or part of this article, use this link http://mct.aacrjournals.org/content/6/2/441. Click on "Request Permissions" which will take you to the Copyright Clearance Center's (CCC) Rightslink site.